Available online at www.sciencedirect.com
ScienceDirect
Journal of Power Sources 170 (2007) 216–224
JOURNAL OF POWER SOURCES
www.elsevier.com/locate/jpowsour

Design of an implantable power supply for an intraocular sensor, using POWER (power optimization for wireless energy requirements)

F. Albano [c], M.D. Chung [d], D. Blaauw [b], D.M. Sylvester [b], K.D. Wise [a,b], A.M. Sastry [a,c,d,*]

[a] *Department of Biomedical Engineering, University of Michigan, Ann Arbor, MI 48109, USA*
[b] *Department of Electrical Engineering and Computer Science, University of Michigan, Ann Arbor, MI 48109, USA*
[c] *Department of Material Science Engineering, University of Michigan, Ann Arbor, MI 48109, USA*
[d] *Department of Mechanical Engineering, University of Michigan, Ann Arbor, MI 48109, USA*

Received 2 March 2007; received in revised form 1 April 2007; accepted 3 April 2007
Available online 11 April 2007

Abstract

The reduction in size and power usage of MEMS (microelectromechanical systems) devices has enabled development of fully implantable medical devices [K.D. Wise, IEEE Eng. Med. Biol. Magaz. 24(5) (2005) 22–29], though major obstacles remain in developing devices of very small scale (<1 mm) [T. Simunic, L. Benini, G. De Micheli, IEEE Trans. Very Large Scale Integr. (VLSI) Syst. 9 (2001) 15–28]. One of the most challenging applications; an intraocular sensor (IOS) developed by the Wireless Integrated Micro-Systems-Engineering Research Center (WIMS-ERC) at The University of Michigan; is the subject of the present study. Our specific objectives are fourfold: (1) to model the power usage of an intraocular sensor (IOS); (2) to develop a methodology for optimization of Hybrid Implantable Power Systems (HIPS); (3) to apply the selection tool to identify candidate power systems; and (4) to establish a methodology to fabricate and test the performance of an optimized power supply. In the present study we fabricated and tested three different cells. For one of these, 10 complete discharge and recharge cycles were successfully obtained. The experimental capacity was 7.70 mAh (15% of theoretical) for a discharge rate of C/5. As part of future work, a microbattery will be built for the WIMS-ERC IOS and tested in a fully integrated testbed.

Keywords: MEMS; Hybrid; Power; Optimization; Implantable; Microbattery

1. Introduction

The reduction in size and power usage of MEMS (microelectromechanical systems) devices has enabled development of fully implantable medical devices [1], though major obstacles remain in developing devices of very small scale (<1 mm) [2]. Power systems typically comprise ∼85% mass and ∼35% volume of these devices, with typical representative applications shown in Table 1 [3–9]. The smallest commercial batteries currently available on the market, with sizes that span the millimeter range, comprise Zinc and Lithium based electrochemistries (Zn-air, Zn/AgO, Li-polymer, Li/MnO_2, etc.). A stainless steel case is typically employed to contain the fluid electrolyte KOH (aq) or the gaseous reaction byproducts. The volume fraction of the case can represent up to 50%, a particularly onerous requirement for implantable technologies.

Further miniaturization of implantable systems will require new battery technologies, compatible with MEMS (microelectromechanical systems) fabrication techniques. One of the most challenging applications an intraocular sensor (IOS) developed by (WIMS-ERC) at The University of Michigan is the subject of the present study. This device has power consumption of $O \sim$ nW, drawing a current of $O \sim$ nA, and other characteristics shown in Table 2.

Indeed, this and other novel implantable biosensors, represent a huge change in the domain of required power for implantable power systems (IPS). The first of these, pacemakers, were developed in the U.S. in the late 1950s [4]. A primary battery, of ∼30 cm^3 in volume and with a 2-year lifetime, was implanted in a stainless steel case. The chest cavity provided sufficient volume for the installation of the large power source. As

* Corresponding author at: Department of Mechanical Engineering, #2140 G.G. Brown Building, University of Michigan, Ann Arbor, MI 48109, USA.
E-mail address: amsastry@umich.edu (A.M. Sastry).

0378-7753/$ – see front matter © 2007 Elsevier B.V. All rights reserved.
doi:10.1016/j.jpowsour.2007.04.007

Nomenclature

C	discharge rate (A); $C/5$ is the current (A) to fully discharge a battery in 5 h
EMT	environmental monitor testbed
HIPS	hybrid implantable power system
HPS	hybrid power system
IOS	intra-ocular sensor
IOS-1	first battery prototype
IOS-2	second battery prototype
IOS-3	third battery prototype
IPS	implantable power system
MEMS	microelectromechanical systems
$O\sim$	Landau notation, $O\sim$ cm^3 = order of cm^3
PDMS	polydimethylsiloxane
POWER	power optimization for wireless energy requirements, a matlab® algorithm
WIMS-ERC	Wireless Integrated Micro-Systems-Engineering Research Center

Table 1
WIMS-ERC IOS specifications

Operating voltage	350 mV
Current draw	12 nA
Power	4.2 nW
Available surface for power	1.28 mm^2 (800 μm × 1600 μm)
Available volume for power	0.256 mm^3 (800 μm × 1600 μm × 200 μm)

secondary cell technology appeared in the 1980s, with the introduction Ni–Cd rechargeable batteries, IPS of smaller volume were produced ($O\sim 10$ cm^3). Coupled with novel electronics technologies, these new power sources enabled development of auditory prostheses [6,8] that could fit within the relatively small volumes available in the human skull. More recent improvements in safety of the Li-ion technology, one of the most energy-dense electrochemistries, have made it a suitable candidate for medical implants. In 2005 a battery of approximately 5 cm^3 was utilized to power a fully implantable spine stimulator [9].

Selection of a power sources relies on more than simply the electrochemistry. Form factor, performance, lifetime, toxicity of the chemicals and the rate of heat generation from the battery must be weighed, particularly in implantable systems. Recently, we have demonstrated a methodology for generating hybrid implantable power systems (HIPS), resulting in increased lifetime and decreased mass and volume (key parameters for implantation) [10,11]. Dual battery systems to address variable rates of discharge have been developed and demonstrated by other groups to be effective in addressing this issue for portable electronics [12] and for select, implantable systems [13].

However, a method for development of a hybrid implantable power system (HIPS) that globally addresses all key constraints (lifetime, mass, volume, variable current draw, etc.) has never been proposed, to the authors' best knowledge. Thus, the goals of this work are to do so, using the WIMS-ERC intraocular sensor (IOS) as a challenge problem (Fig. 1). Our specific objectives are fourfold:

(1) To model the power usage of an intraocular sensor (IOS);
(2) To develop a methodology for optimization of HIPS;
(3) To apply the selection tool to identify candidate power systems; and
(4) To establish a methodology to fabricate and test the performance of optimized anode and cathode couple.

Packaging optimization is reserved for future work. Our work spanned experimental and theoretical efforts, described in the next section.

2. Methods

In order to meet clinical goals, an IOS must be implanted within the eye, and continuously monitor pressure, for the entire period of treatment of a patient suffering from glaucoma. Treatment times vary, but are at most 2 years. During this time, a power supply is subject to a constant voltage and a constant current draw.

We utilized our code POWER to select the most suitable electrochemistry/ies and to determine the best cell configuration for this application. The input values for the code are reported in Table 3. To have a conservative evaluation we introduced a current draw for the optimization code around three orders of magnitude (10^3) higher than the one specified by the WIMS-ERC for this application.

The power profile of an IOS was determined by considering the device current draw specified by the WIMS-ERC and by coupling it with a patient daily routine. The device draws a constant current of approximately 12.0 nA when activated, and a negligible current when kept in a sleep mode (∼1 nA). We estimated the active portion of the duty cycle to be 16 h. Once our code selected a suitable electrochemistry, theoretical val-

Table 2
Evolution of implantable batteries and clinical trials [4–9]

Application	Electrochemistry	Clinical test	Location	Year
Pacemaker	Zinc–mercury	Dogs and humans	USA	1958–1959
Biotelemeter (monitoring device)	Nickel–cadmium	Dogs	USA	1982
MEI (middle ear implant)	Primary MnO_2/Li secondary Ni–Cd	Humans	JAPAN	1988
Ventricular assist device, artificial heart	Li-ion	Calves, pigs, human cadavers	USA	1995
TICA (hearing prosthesis)	Secondary Ni–Cd	Cats, dogs, humans	GERMANY	1998
Spinal cord OFS (oscillatory field stimulator)	Secondary Li-polymer	Rodents, dogs, humans	USA	2005

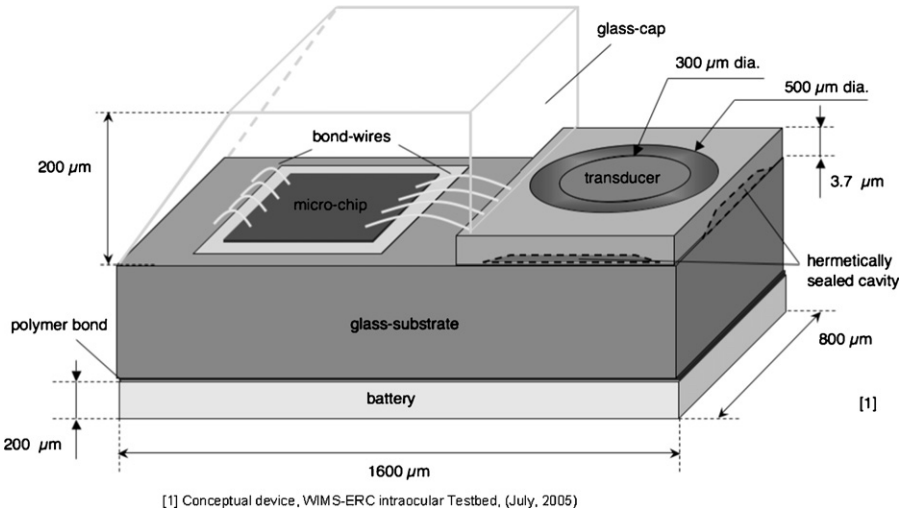

Fig. 1. Schematic of WIMS-ERC IOS.

ues for voltage and capacity from the chemical reactions were calculated. Because these values calculated can be significantly higher than practically achievable values, appropriate correction factors were included (typically 40% of the theoretical value is the actual capacity [14]). Calculated voltage and capacity were used to help identify candidate materials, and to estimate of lifetime.

We proposed fabrication of a microbattery utilizing zinc and silver as electrode materials. Our battery database was adapted for the IOS case study by including cells with a flat discharge profile suitable for this kind of power draw, particularly Zn/AgO. For comparative purposes, a Ni/Zn secondary cell from Bipolar Technologies [15,16] was also added to our database to be employed as a primary cell. A comparison of these electrochemistries is given in Table 6. Because of the rather short lifetime required by this application ($\leq$2 years), rechargeability was not taken into account in the POWER computation of the number of operation cycles provided by the battery. We investigated rechargeability of the batteries during our experimental evaluation, however, for the purpose of having different prototypes of batteries; we further felt it demonstrated system robustness.

We used POWER to identify suitable candidate commercial batteries. The version of the database used in this study comprised 194 primary batteries, including Zn/AgO, Ni/Zn, Zn/MnO_2, Alkaline, Lithium and Li/MnO_2 electrochemistries. The primary constraints were the size and shape (volume and form factor) and mass of the batteries. The secondary constraint was the implantability of the system. Electrochemistries that have been previously tested in mammals and humans clinical studies (Table 2) were targeted.

In the present study we fabricated and tested three different cells, which we will refer to as IOS-1, IOS-2 and IOS-3 throughout the paper. The first battery, IOS-1, was designed to establish that a completely functional battery could be fabricated and sealed, starting from a commercial system. The second battery, IOS-2, was fabricated to investigate the effects of electrolyte fill inside the reaction chamber, and to determine if the cell could be recharged. The third battery, IOS-3, was designed to asses the effects of scaling down the battery system to the submillimeter size required by the application.

Battery IOS-1 was produced by resizing a Renata 317 Zinc/Silver oxide coin cell. The original cell has a diameter of 7.60 mm and a thickness of 1.56 mm. Using a Dremel® tool we removed the outer stainless steel case of the original cell. Anode, cathode, separator and sealing ring were collected. Current collectors were cut from a tin (Sn) foil into a shape suitable to contain the anode and cathode, and for connection of leads. Macor® ceramic (see Table 4 for chemical composition [17]) was utilized as material for building the battery package. Several battery half-packages were used, which had been fabricated from a 3.0 in. × 3.0 in. tile of Macor® ceramic. Two round half-packages of inner diameter ~2.5 mm and outer diameter ~4.5 mm, with masses of ~0.05 g each, were selected, among the previously produced samples, to hold anode and cathode materials, respectively. The electrodes were resized to fit an approximate area of ~4.9 mm^2 (corresponding to a half-package

Table 3
Input parameters for POWER

Operating voltage	350 mV
Current draw	15 μA
Electrochemistry (primary/secondary)	Primary
Prioritization (mass/volume)	Mass
Number of power sites	2
Operation time	16 h

Table 4
Macor® ceramic composition [17]

Compound	Approximate weight (%)
Silicon, SiO_2	46
Magnesium, MgO	17
Aluminium, Al_2O_3	16
Potassium, K_2O	10
Boron, B_2O_3	7
Fluorine, F	4

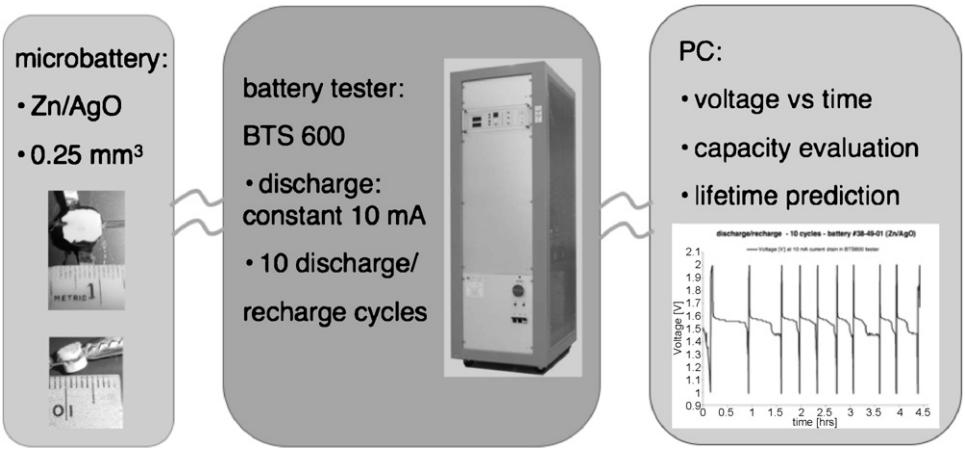

Fig. 2. Schematic of the battery discharge setup.

footprint) and a polypropylene separator membrane (DuPont® spunbonded polypropylene [18]) measuring ∼4.0 mm^2 was dissected.

The battery was then assembled. The first half-package was filled, with a current collector (Sn), the cathode material (AgO) and the polypropylene separator membrane (DuPont® spunbonded polypropylene [18]). The second half-package was filled, with a current collector (Sn) and the anode material (Zn). The two half-packages were then flooded with the electrolyte, a solution of potassium hydroxide (28% KOH, 1% Li, from Yardney Technical Products Inc.). Using two parts epoxy resin (Emerson & Cuming type Stycast 2850FT black [19]), the package was sealed immediately, and was set to cure into a Plexiglass clamp for 24 h. Rubber (PDMS) pads were used to distribute the load on the package and prevent cracking. Masses of active materials were not measured for this first cell, and thus theoretical capacity estimates were made after the package was sealed based on the approximate battery volume of 4.9 mm^3. Once the battery was sealed, it was discharged at a constant load of ∼11 MΩ. The discharge current was measured using a Keithley current meter type 6517A. The discharge setup is described by the schematic in Fig. 2; data were collected using a National Instruments acquisition card type 6035E.

Battery IOS-2 was produced using two cells type Renata 317, and tested according to the same procedure. A package was prepared by machining two pieces of Macor® ceramic, Figs. 3a and b detail its geometry. Inlet and outlet channels were built into the package using a glass microtube, type μTIP^{TM}-TIP5TW1 from WPI, as shown in Fig. 4. The mass of active material was recorded, and used to estimate theoretical capacity. The first half-package was filled with a current collector (Sn), 0.069 g of the cathode material (AgO), and polypropylene separator membrane (DuPont® spunbonded polypropylene [18]). The second half-package was filled with a current collector (Sn), and 0.026 g of anode material (Zn). Using two parts epoxy resin, Stycast 2850FT black, the package was sealed and cured in a Plexiglass clamp for 24 h. No electrolyte was inserted into the package, and air was able to flow through the glass tubes. After the package was fully cured, electrolyte (28% KOH, 1% Li, from Yardney Technical Products Inc.) was inserted using an Eppendorf EZ-pet automatic pipette as a pumping device.

After ∼3cm^3 of electrolyte were allowed to flow through the battery using the pipette, the inlet and outlet channels were closed using PDMS stoppers. The battery was then discharged and the voltage was recorded. Once the voltage initially dropped below 1.1 V additional electrolyte was pumped into the battery under discharge, using the automatic pipette. After the

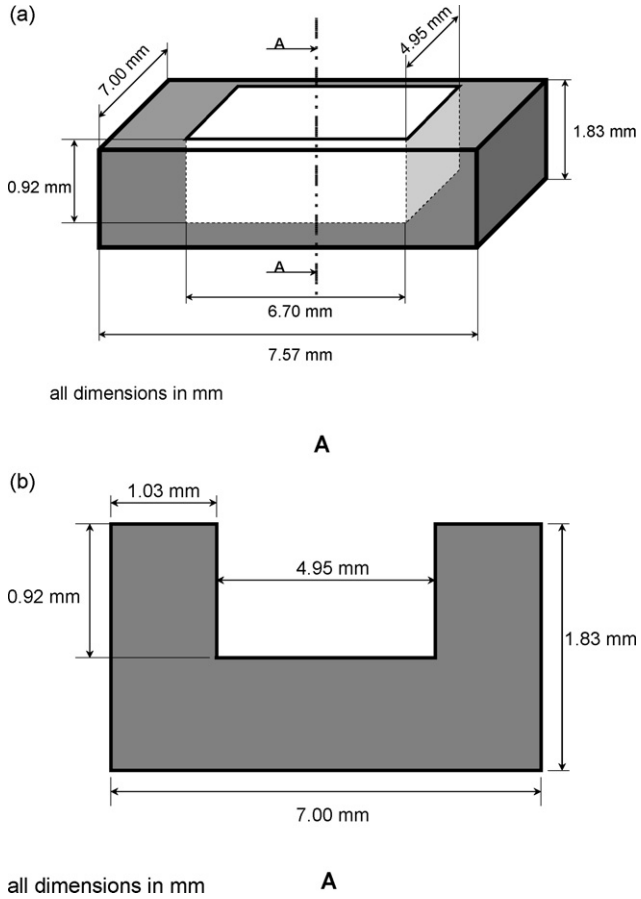

Fig. 3. (a) Dimensions of IOS-2 package. (b) Dimensions of IOS-2 package (section A–A).

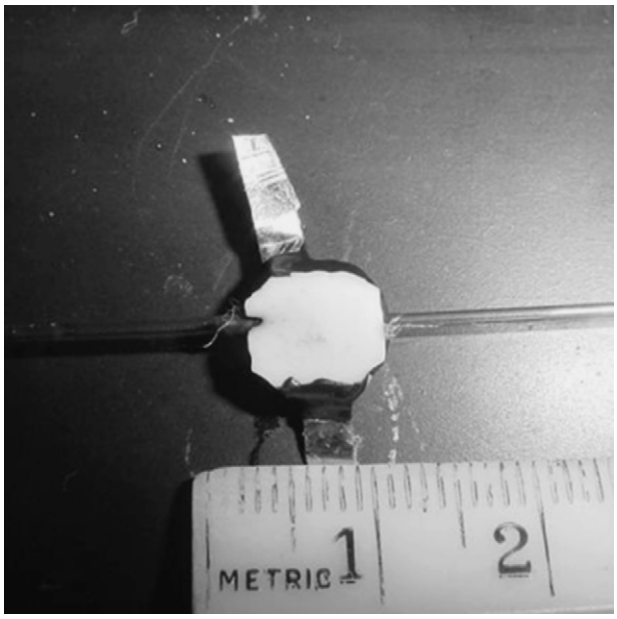

Fig. 4. IOS-2 showing inlet and outlet glass tubes.

voltage dropped a second time below 1.1 V, the battery was disconnected and additional electrolyte was inserted. After this operation, voltage was recorded and the battery was cycled for 10 discharge/recharge cycles using a Firing Circuits battery tester type BTS600. The discharge voltage lower limit was set to 1.0 V and the recharge voltage limit was set to 2.0 V.

Battery IOS-3 was produced using another Renata 317 cell, and tested as before. The mass of active material was recorded, and used to estimate theoretical capacity. For this cell current collectors were cut from a copper (Cu) foil. Two round Macor® ceramic packages of inner diameter ∼1.5 mm and outer diameter ∼4.5 mm, with masses of ∼0.05 g each, were used for the external structure. The first half-package was filled with a current collector (Cu), 0.0040 g of the cathode material (AgO), and polypropylene separator membrane (DuPont® spunbonded polypropylene [18]). The second half-package was filled with current collector (Cu) and anode material (Zn) in the amount of 0.0060 g. The battery was again discharged according to the same procedure.

3. Results

In Table 5 we report the results of our optimization routine (POWER). All three approaches selected a Zn/AgO commercial system from the database. Approach 1 selected a battery type Renata #364, with a mass of 0.32 g and a volume of ∼78.0 mm^3. Approach 2 provided only one solution in the micro-power range (μW), selecting a battery type Maxell #SR421SW having a mass of 0.17 g and a volume ∼39.0 mm^3. Approach 3 selected a battery type Renata #337 for each one of the two specified power sites presenting a mass of 0.12 g and a volume of ∼30.0 mm^3. The resulting projected lifetimes of all three approaches exceeded the targeted lifetime (2 years), by more than three orders of magnitude.

With the specified power requirements and volume constraints (Table 1) a nickel electrochemistry provides a lifetime of 0.64 years (∼40% of theoretical, per [14]) not accounting for rechargeability, while a silver electrochemistry provides a lifetime of 3.63 years (∼40% of theoretical, per [14]). We report detailed theoretical calculations in Table 6.

In Fig. 5 we report the discharge profile for battery IOS-1. The output voltage measured after the battery was fabricated and connected to the discharge setup (Fig. 2) was ∼1.5 V. The cutoff voltage for the discharge test was set to 0.8 V. The initial current draw was 136.0 nA. From the discharge profile (Fig. 5) we estimate the cell capacity. For this estimate, we select a cutoff voltage of 1.11 V, corresponding to a time of 6.7 h of operation. Thus the experimental capacity for battery IOS-1 was 0.67 μAh. Based on the 4.9 mm^3 cell volume we extrapolate a theoretical capacity of 1.7 mAh, for an energy density of 525 Wh L^{-1} [14].

In Fig. 6 we report the discharge profile for battery IOS-2. The output voltage measured after the battery was fabricated and connected to the discharge setup (Fig. 2) was ∼1.5 V. The cutoff voltage for the discharge test was set at ∼1.1 V. The initial current draw measured was 136 nA. The voltage profile shows the effect of the electrolyte depletion from the reaction chamber due to lack of hermetic seal. After new electrolyte was inserted, a new peak of ∼1.6 V was recorded.

After battery IOS-2 reached a voltage of 1.1 V for the second time, we investigated rechargeability; results are reported in Fig. 7. The battery was cycled 10 times at a current draw

Table 5
Results of POWER analysis[a]

	Manufacturer	Part no.	Electrochemistry	Total no.	No. of cycles (no battery re-charge)	Total mass (g)	Total volume (cm^3)
Approach 1	Renata	364	Zn/AgO	1	2.21E+06	3.20E−01	7.81E−02
Approach 2							
Micro	Maxell	SR421SW	Zn/AgO	1	2.13E+07	1.70E−01	3.89E−02
Totals				1	2.13E+07	1.70E−01	3.89E−02
Approach 3							
Site 1	Renata	337	Zn/AgO	1	2.99E+04	1.20E−01	2.99E−02
Site 2	Renata	337	Zn/AgO	1	2.99E+04	1.20E−01	2.99E−02
Totals				2		2.40E−01	5.98E−02

[a] WIMS-ERC (IO testbed-mass priority 16 h of operation).

Table 6
Theoretical calculations for Ni/Zn and Ag/Zn electrochemical couples [14,16,27–29]

Electrochemical couple	Ni/Zn	Ag/Zn
Theoretical voltage	1.73 V	1.5 V
Specific energy	100–120 mAh g^{-1}	500 mAh g^{-1}
Commercial cell specific energy	37.5 mAh g^{-1}	29–76 mAh g^{-1}
Commercial cell energy density	106 mAh cm^{-3}	48–142 mAh cm^{-3}
Commercial cell capacity	0.03 mAh	20–180 mAh
Commercial cell additives	Unknown	Unknown
Theoretical capacity of a 0.25 mm^3 cell	0.17 mAh	0.94 mAh
Effective capacity of a 0.25 mm^3 cell	0.026 mAh (commercial cell)	0.012–0.035 mAh (commercial cell)
Theoretical lifetime at 12 nA discharge current	1.6 years	9.0 years
Effective lifetime at 12 nA discharge current	0.25 years (∼3 months)	0.34 years (∼4 months)

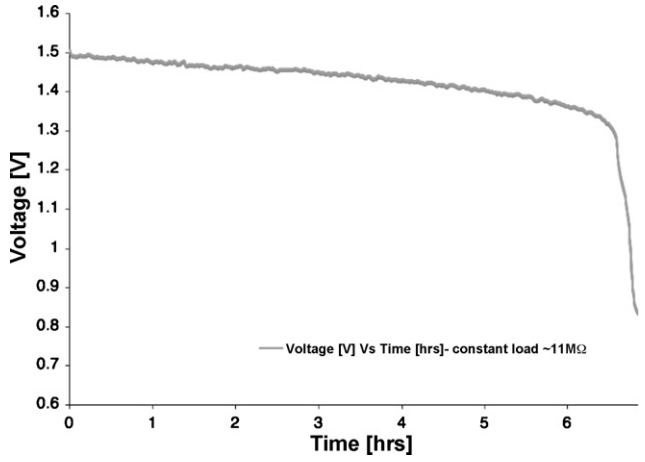

Fig. 5. Discharge profile for IOS-1.

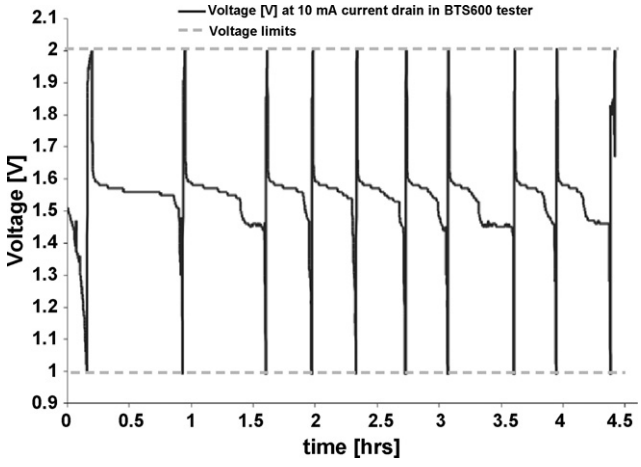

Fig. 7. Discharge and recharge profiles for 10 cycles IOS-2.

of 10 mA, which corresponds to a rate of *C*/5. The 10 cycles were run over approximately 4.5 h. From the first discharge cycle (Fig. 7), we estimate the experimental capacity of cell IOS-2 to be ∼7.7 mAh, and we evaluate the theoretical capacity based on the mass of the active materials as follows. The anode material (Zn) has a specific capacity of 0.82 Ah g^{-1} [14], thus 0.026 g utilized theoretically produced 21 mAh. The cathode material (AgO) has a specific capacity of 0.43 Ah g^{-1} [14], thus the 0.069 g introduced theoretically produced 30 mAh. Therefore, the overall cell theoretical capacity was calculated to be 21 mAh.

In Fig. 8 we report the discharge profile for battery IOS-3. As before the initial voltage was ∼1.5 V; the test was terminated at a voltage ∼1.2 V. From the discharge profile (Fig. 8), we estimate an experimental capacity of 0.69 μAh, while we used the masses of active materials to evaluate the theoretical capacities. Battery IOS-3 was built using a package of ∼0.56 mm^3,

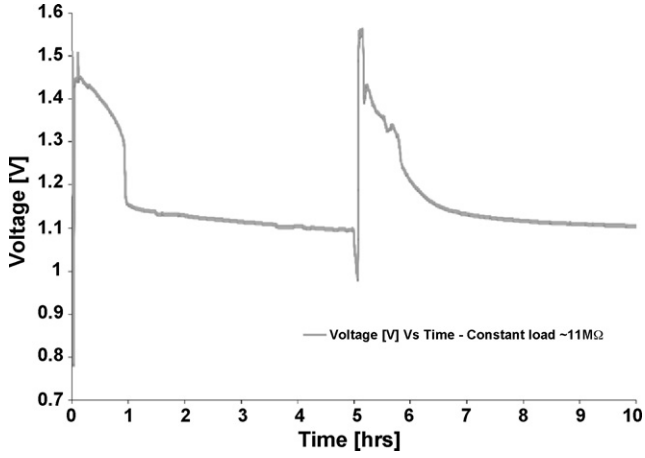

Fig. 6. Discharge profile for IOS-2, showing the effect of electrolyte insertion during discharge.

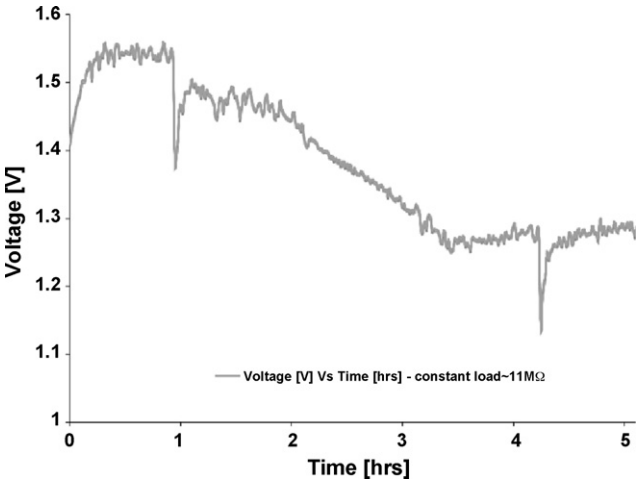

Fig. 8. Discharge profile for IOS-3.

Table 7
Characteristics and performance of IOS-1, IOS-2 and IOS-3 comparison

Battery no.	Volume (mm^3)	Theoretical capacity	Experimental capacity	Projected lifetime (as a primary cell) at 12 nA draw
IOS-1	∼4.9	1.7 mAh	0.67 μAh	56 h
IOS-2	∼60	21 mAh	7.7 mAh	73 years
IOS-3	∼0.56	1.7 mAh	0.69 μAh	57 h

i.e. approximately 1/10 that of battery IOS-1. The amount of anode (Zn) material utilized for this battery was 0.0060 g providing a theoretical capacity of 4.9 mAh. The amount of cathode (AgO) material employed for this cell was 0.0040 g, providing 1.7 mAh. Overall, the calculated theoretical capacity for battery IOS-3 was 1.7 mAh. We attempted to recharge the battery using a 1.5 V alkaline commercial cell but the original voltage was not reached and the cell self-discharged.

In Table 7 we summarize the projected lifetime for the batteries produced in this study as calculated by dividing the cell experimental capacity by the specified discharge current (12 nA). Microbatteries IOS-1 and IOS-3 achieved the projected lifetime of more than 50 h, while microbattery IOS-2 shows a projected lifetime one order of magnitude above the required 2 years; cell volumes (mm^3) and capacities (Ah) are also presented in Table 7.

4. Discussion

Promising steps towards the reduction in sizes of power supplies have been made, through application of lithographic techniques [20], thin-film technology [21] and rechargeable and caseless designs [22,23]. Yet, the size reductions achievable through use of secondary versus primary systems, or thin film versus thicker electrodes, are actually less than those attainable simply by employing a hybrid architecture. Indeed, combining these strategies appears to be the most promising route.

Such hybrid systems have been developed for a variety of applications, often with excellent results in reduction of total system size and mass. A hybrid battery system comprised of two cells, a 6.0 V $LiMnO_2$ and a 3.0 V Li-iodine cell was proposed to replace the existing power supply of a defribillator cardioverter [13]. The new system presented a ∼15% reduction in volume and ∼5% reduction in mass, compared to the original unique battery (a bigger 6.0 V $LiMnO_2$ cell), while the capacity increased by ∼40%. A hybrid system composed by a battery and a solar cell was proposed [24] to power a generic multielement microsystem for portable wireless applications [25]. The concept system resulted in a theoretical size reduction of ∼98% compared to using just one custom-fabricated battery. The solution to the challenges posed by the power demands of MEMS devices such as the WIMS-ERC EMT [10] or the WIMS-ERC Amadeus cochlear implant [11] were only possible by applying a hybrid approach, combining primary and secondary systems, high energy and power dense systems.

Though the prototype batteries produced in the present study do not yet meet the small scale required for the WIMS-ERC IOS of 1600 μm × 800 μm × 200 μm, they did provide proof-of-concept on capacity and lifetime. In order to achieve the small size required, reduction in packaging will be required. Caseless battery systems have been proposed [22,23] for implantable MEMS applications. The Mg/AgCl and Mg/CuCl batteries [22] comprised minimum volumes of ∼144 mm^3 and had capacity of 1.8 mWh; if scaled down to the 0.256 mm^3 required by the present application, the theoretical lifetime at 12 nA would be ∼30 days. Even if the lifetime could be increased, our main concern with implanting this system without a casing is inherent risk in the pressure build up that hydrogen bubbles in Mg/AgCl systems can produce [22]. The Zn/AgCl system proposed by the second group comprised a volume of ∼0.1 mm^3, which would be suitable for the present geometry, yet the lifetime at 12.0 nA would be only ∼4 h, making it unsuitable for the present application. The glucose/O_2 systems proposed, capable of providing a tenfold increase in energy density, and consequently lifetime (5000 Wh L^{-1} versus 500 Wh L^{-1} of Zn/AgCl system [23]), are based on a cathode material (bilirubin oxidase) that is not stable [23]. It seems very unlikely, given potential toxicity, that stabilizing additives (mainly heavy metals) could be used in these systems without a package.

The IOS-1 cell capacity (0.67 μAh, estimated at 1.11 V cutoff voltage after 6.71 h of discharge under a current draw of 136.0 nA) was significantly less than the theoretical capacity of 1.7 mAh (based on an energy density of 525 Wh L^{-1} [14]). This four order-of-magnitude difference was likely the result of several well-known factors. One of these is likely incomplete filling with electrolyte. Another factor is related to the electrodes design, the reduced size of the electrodes (∼4.9 mm^2) and their flat geometry only allow limited active material surface area to be accessible to the electrolyte.

Batteries IOS-1 and IOS-3 achieved 0.01% of theoretical capacity, while battery IOS-2 achieved 15%, as calculated by multiplying the discharge current by the discharge time required to reach the cutoff voltage (reported in Table 7). This latter result compares favorably with other microbatteries in the literature. For example, Ni/Zn microbatteries and Li thin film batteries, which have achieved which have achieved ∼7% [16] and ∼12% [21] of theoretical capacity, respectively. Losses occur because of capacity fade related to the discharge rate, low surface area of active material and lack or depletion of the electrolyte. Clearly, work is needed on identifying the optimum discharge rate, on improving the morphology of the active material and on achieving and preserving 100% full electrolyte within the reaction chamber.

Electrolyte management remains a challenge for other, operational reasons in addition to its role in loss of capacity. Not only is electrolyte insertion difficult because of the reduced size of the package, but it is practical only before the package is sealed, and complicated by capillary forces. In Fig. 6 we show how

the addition of new electrolyte restores the initial value of the voltage for cell IOS-2. This result shows how a complete fill of the reaction chamber with electrolyte is fundamental to obtain a capacity value closer to nominal. Moreover the inlet and outlet channels in cell IOS-2 allowed better control of the amount of electrolyte inserted into the cell casing. The voltage drop in Fig. 6 is entirely due to the electrolyte depletion, and not to actual discharge since the starting voltage was completely restored by the operation of replenishing electrolyte into the chamber.

The cell lifetime (>50 h for IOS-1 and IOS-3), estimated in Table 7 (by dividing the cell experimental capacity by the specified discharge current, 12.0 nA) was significantly less than the theoretical one (60–80 years). Similarly, for IOS-2, the actual lifetime was only 10% of the theoretical. This compares favorably with other microbatteries in the literature (Zn miniature batteries [23] projected a lifetime of 2–4 weeks, i.e. 2% of similar commercial systems lifetimes (1–3 years); Ni/Zn and Li-ion microbatteries [26] achieved ∼25% increase in lifetime due to electrolyte management and sealing). Microbattery IOS-3 showed a capacity, and consequently a lifetime, comparable to IOS-1, even with a size ∼10 times smaller, because of the efficient electrolyte filling and package seal. Lower lifetimes resulted from capacity fade related to the discharge schedule and depletion of the electrolyte. Clearly, work is needed on identifying the optimum discharge schedule of our system and on improving the electrolyte management and package seal. Battery IOS-2 achieved a projected lifetime (without recharge) ∼30 times higher than required. This is mainly due to the larger size and capacity of this cell, but is also related to the fabrication technique. A complete electrolyte fill of the reaction chamber enabled a higher output capacity. The cycling test for IOS-2 was run for approximately 4.5 h, and produced 10 cycles of discharge/recharge. For determining the actual cycle life of this battery, which was not an objective of the present paper, extensive cycling tests will be required.

5. Conclusions/future work

Our study demonstrated the feasibility of design and construction of a microbattery, by optimizing both geometry and electrochemistry through careful analysis of a load profile. We developed Zn/AgO fabrication technique, demonstrated for three prototype cells: IOS-1, IOS-2 and IOS-3. Cells volumes were ∼4.9, ∼60 and 0.56 mm^3, respectively, with experimental capacities of 0.67, 7.7 and 0.69 μAh (see Table 7). The original commercial system (Renata 317) had a volume of 43.6 mm^3 of and a nominal capacity of 10.5 mAh.

Cells IOS-1 and IOS-3 were discharged at 136 nA; cell IOS-2 was discharged at both 136 nA and 10 mA. Ten complete discharge and recharge cycles were successfully obtained for cell IOS-2. Package size reduction is a key objective to achieve in order to integrate the battery with the IOS and make it an IPS. In order for this battery to be implanted a perfect seal of the package is required. In the present work, we studied the effects of package seal and electrolyte depletion on cell rechargeability and lifetime, but we have not yet investigated the durability of the seal for long-term implantation.

Compared to other microfabricated power systems, these Zn/AgO cells present a higher energy density and a flatter discharge curve, which makes them suitable for MEMS applications. By refining the fabrication techniques and cell design developed in this study, it should be possible to build batteries that have a longer lifetime. At present, the microbatteries do not yet meet the rigorous volume requirements (0.256 mm^3) of the IOS; the smallest of our prototypes (IOS-3) is ∼50% bigger than the required size. Mass constraints have also been neglected in the current work. The present package of IOS-3 (∼0.1 g) comprises almost 80% of the battery total mass.

The capability to recharge this electrochemistry can extend the ultimate lifetime of the device and allow a longer permanent implantation. Future work will entail continued evaluation of the hermetic package seal, while also consideration of reduction of mass. At present, a set of microbatteries is being constructed for a fully integrated testbed, to assess their nominal capacity and effective lifetime.

Acknowledgements

We acknowledge helpful discussion with Prof. Yogesh Gianchandani on packaging in this work. Sponsorship of this effort was primarily from the Engineering Research Centers program of the National Science Foundation under NSF Award Number EEC-9986866; support for some of the facilities used in this project was provided by the Assistant Secretary for Energy Efficiency and Renewable Energy, Office of FreedomCAR and Vehicle Technologies of the U.S. Department of Energy under contract No. DE-AC02-05CH11231, subcontract No. 6720903.

References

[1] K.D. Wise, IEEE Eng. Med. Biol. Magaz. 24 (5) (2005) 22–29.
[2] T. Simunic, L. Benini, G. De Micheli, IEEE Trans. Very Large Scale Integr. (VLSI) Syst. 9 (2001) 15–28.
[3] W. Greatbatch, J. Med. Eng. Technol. 8 (1984) 56–63.
[4] W. Greatbatch, Pace 7 (1984) 143–147.
[5] D.C. Jeutter, IEEE Trans. Biomed. Eng. 29 (5) (1982) 314–321.
[6] H. Ikeda, N. Furukawa, S. Narukawa, S. Yoshizawa, Adv. Audiol. 4 (1988) 73–84.
[7] T. Mussivand, A. Hum, M. Diguer, K.S. Holmes, G. Vecchio, R.G. Masters, P.J. Hendry, W.J. Keon, Biosens. Bioelectron. 11 (1996) IV.
[8] J.W. Baumann, H. Leysieffer, Hno 46 (2) (1998) 121–128.
[9] S. Shapiro, R. Borgens, R. Pascuzzi, K. Roos, M. Groff, S. Purvines, R.B. Rodgers, S. Hagy, P. Nelson, J. Neurosurg.-Spine 2 (2005) 3–10.
[10] K.A. Cook, A.M. Sastry, J. Power Sources 140 (1) (2005) 181–202.
[11] K.A. Cook, F. Albano, P. Nevius, A.M. Sastry, J. Power Sources 159 (1) (2005) 758–780.
[12] Q. Wu, Q. Qiu, M. Pedram, in: IEEE (Ed.), Proceedings of the Asia and South Pacific Design Automation Conference, Yokohama, Japan, 2000, pp. 387–390.
[13] J. Drews, R. Wolf, G. Fehrmann, R. Staub, J. Power Sources 80 (1999) 107–111.
[14] D. Linden, T.B. Reddy, Handbook of Batteries, 3rd ed., McGraw-Hill, New York, 2002, p. 12.1.
[15] http://www.bipolartechnologies.com/Microbattery2.htm, accessed February 7, 2007.
[16] P. Singh, X.Q. Wang, R. LaFollette, D. Reisner, Proc. IEEE Sens. 1–3 (2004) 349–352.

[17] http://www.corning.com/docs/specialtymaterials/pisheets/Macor.pdf, accessed January 28, 2007.
[18] http://www2.dupont.com/Separation_Solutions/en_US/tech_info/spunbonded/spunbound_poly.html, accessed February 16, 2007.
[19] http://www.emersoncuming.com/other/2850ft.pdf, accessed February 7, 2007.
[20] P.H. Humble, J.N. Harb, R.M. LaFollette, J. Electrochem. Soc. 148 (2001) A1357–A1361.
[21] B.J. Neudecker, N.J. Dudney, J.B. Bates, J. Electrochem. Soc. 147 (2000) 517.
[22] F. Sammoura, K.B. Lee, L. Lin, Sens. Actuators A: Phys. 111 (1) (2004) 79–86.
[23] A. Heller, Anal. Bioanal. Chem. 385 (2006) 469–473.
[24] J.N. Harb, R.M. LaFollette, R.H. Selfridge, L.L. Howelld, J. Power Sources 104 (1) (2002) 46–51.
[25] A. Mason, N. Yazdi, A.V. Chavan, K. Najafi, K.D. Wise, Proc. IEEE 86 (1998) 1733–1746.
[26] R.M. LaFollette, J.N. Harb, P. Humble, Sixteenth Annual Battery Conference on Applications and Advances, 2001, pp. 349–354.
[27] http://www.powergenixsystems.com, accessed October 7, 2005.
[28] http://www.yardney.com, accessed October 7, 2005.
[29] http://www.duracell.com/procell/chemistries/silver.asp, accessed October 3, 2005.